ISSN 1063-7826, Semiconductors, 2014, Vol. 48, No. 10, pp. 1363–1369. © Pleiades Publishing, Ltd., 2014.
Original Russian Text © Sh.A. Mirsagatov, I.B. Sapayev, 2014, published in Fizika i Tekhnika Poluprovodnikov, 2014, Vol. 48, No. 10, pp. 1398–1404.

PHYSICS OF SEMICONDUCTOR DEVICES

Injection Photodiode Based on a *p*-Si–*n*-CdS–n^+-CdS Structure

Sh. A. Mirsagatov^ and I. B. Sapayev

Physical–Technical Institute, Scientific Production Association "Physics–Sun", ul. G. Mavlyanov 2b, Uzbekistan Academy of Sciences, Tashkent, 100084 Uzbekistan

^ e-mail: mirsagatov@uzsci.net; mohim@inbox.ru

Submitted June 20, 2013; accepted for publication March 14, 2014

Abstract—An injection photodiode with a high room-temperature rectification factor (10^5) is developed based on a *p*-Si–*n*-CdS–n^+-CdS structure. It is shown that the light and dark current–voltage characteristics of the structure have identical features. It is found that the mode of "long" diodes is implemented in the structure at current densities of $I = 10^{-2}$–5×10^{-4} A/cm^2; in this case, the integral (S_{int}) and spectral (S_λ) sensitivities sharply increase. It is shown that $S_{int} = 2.8 \times 10^4$ A/lm (3×10^6 A/W) for an illuminance of $E = 0.1$ lux and $S_\lambda = 2.3 \times 10^4$ A/W under laser irradiation with $\lambda = 625$ nm and a power of $P = 10$ μW/cm^2 at a bias voltage of $V = 20$ V. It is shown that the mechanism of photocurrent amplification is predominantly associated with ambipolar carrier-mobility modulation.

DOI: 10.1134/S1063782614100212

1. INTRODUCTION

There are published works that contain information on the development of injection photodiodes based on II–VI compounds, in particular, cadmium sulfide [1], telluride, and its solid solutions [2–4]. In [1], a Ni–*n*-CdS–n^+-CdS structure based on CdS single crystals was considered. Photocurrent amplification in it under vultra-violet (UV) illumination ($\lambda =$ 0.22 μm) is possible if the level of majority carrier injection to the high-resistivity *n*-type region from the inactive (not illuminated) side of the n^+–*n* junction is increased. Therefore, it is of interest to develop a photodetector with a photosensitivity range spanning a broad spectrum of electromagnetic radiation. Such an injection photodetector with improved output parameters can be developed based on *p*–*i*–*n* structures in which the double injection mode is implemented. However, it is technologically difficult to obtain *p*-type conductivity and *p*–*i*–*n* structures on II–VI compounds, including CdS, due to the self-compensation effect. To this end, we fabricate a *p*-Si–*n*-CdS–n^+-CdS structure with a heterojunction. There the high-resistivity heavily compensated weak *n*-type CdS layer plays the role of an *i* layer. The development of a *p*-Si–n^+-CdS heterojunction is chosen, since it is described in publication [5]. Furthermore, silicon is a well studied material. These reasons are the basis for developing a *p*–*i*–*n* structure based on cadmium sulfide films with a *p*-Si–*n*-CdS heterojunction.

2. SAMPLES AND EXPERIMENTAL

The photosensitive *p*-Si–*n*-CdS–n^+-CdS structure was fabricated by sputtering CdS powders (in a quasi-closed system in a vacuum chamber with a residual pressure of 10^{-5} Torr) onto the surface of a *p*-type silicon wafer 300 μm thick with a resistivity of $\rho \approx$ 10 Ω cm. In this case, the source (CdS) temperature is $T_s \approx 800$–850°C; the substrate (*p*-Si) temperature was maintained within ~250–270°C. The study using a MII-4 microscope showed that CdS films grown on *p*-Si substrates consist of columnar crystallites (grains) oriented in the film-growth direction and misoriented with respect to the azimuth. It was found that the crystallite size greatly depends on the technological conditions, most of all, on the Si substrate temperature. For example, the crystallite size in the CdS films grown at $T_s = 300$°C was ~3–4 μm; crystallites completely penetrated throughout the film thickness $w \approx 2$ μm. The grown CdS films were high-resistivity ($\rho \approx (2$–$3) \times 10^{10}$ Ω cm) with weak *n*-type conductivity. Then, an n^+-CdS film ~50 Å thick was grown on the CdS film and a current-collecting Π-shaped contact was formed by the vacuum evaporation of In.

The current–voltage (*I*–*V*) characteristics of the fabricated *p*-Si–*n*-CdS–n^+-CdS structures were measured in the forward and reverse current directions in the dark and under illumination at an illuminance of $E = 0.1$–100 lux and at room temperature. The structures were illuminated by an LG-75 laser with a radiation power of 10 μW/cm^2–0.75 mW/cm^2 with a wavelength of 0.625 μm, and by an incandescent lamp whose parameters almost correspond to the reference lamp, whose electromagnetic radiation power in one lumen in the visible region of the spectrum is 9.1×10^{-3} W [6]. The spectral dependence of the structure photosensitivity was measured using a 3MR-3 monochromator at room temperature $T = 300$ K. The radiation source was a DKSSh-1000 xenon lamp operating in the minimum acceptable power mode. The lamp provided a

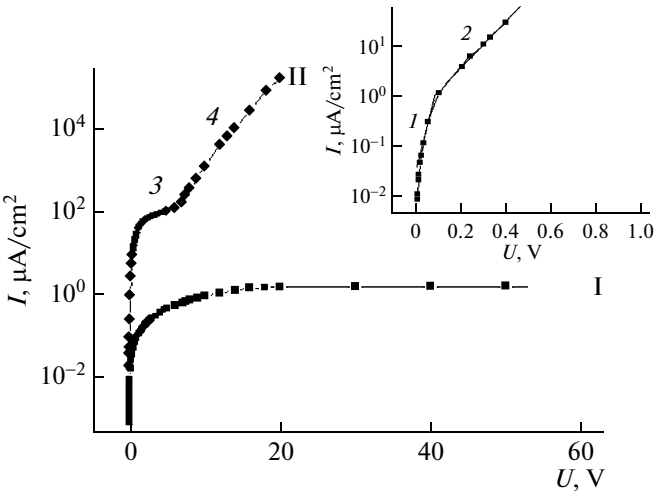

Fig. 1. Semilog current–voltage characteristic of structure in the dark: (I) forward portion in which the (*3*) third and (*4*) fourth portion are indicated; the inset shows the (*1*) first and (*2*) second portions; (II) reverse portion.

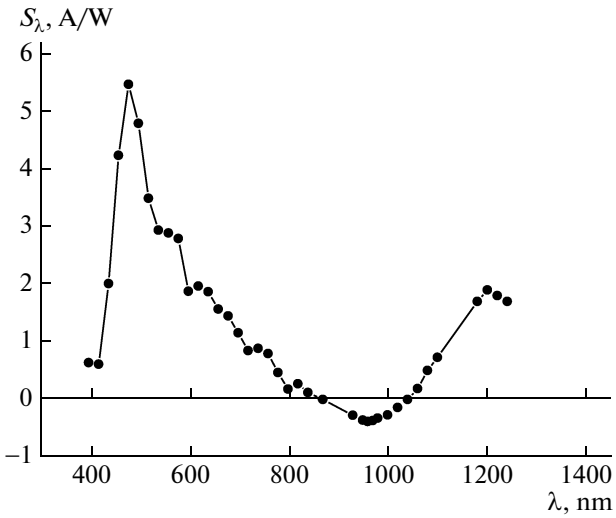

Fig. 2. Spectral distribution of the photosensitivity (S_λ) of the *p*-Si–*n*-CdS–n^+-Cd structure without bias.

light flux of 53000 lm and a brightness up to 120 μMcd/m^2 at the light-spot center. The lamp radiation was calibrated in absolute units using an RTE-9 thermoelement with a quartz window. The DKSSh-1000 lamp has a continuous spectrum in the ultraviolet and visible regions.

3. EXPERIMENTAL RESULTS AND DISCUSSION

Figure 1 shows the semilog forward and reverse portions of the *I–V* characteristic of typical *p*-Si–*n*-CdS–n^+-CdS structures. The cases where the "+" or "–" potential is applied to the *p*-Si contact are considered as the forward or reverse current direction in the structure. An analysis of the *I–V* characteristic shows that the structure has rectifying properties, and its rectification factor K (defined as the ratio of forward and reverse currents at a fixed voltage $V = 20$ V) is ~10^5.

3.1. Spectral Distribution of the Photosensitivity

Figure 2 shows the spectral distribution of the photosensitivity S_λ in the absence of bias voltage. An analysis of the spectral distribution of the photosensitivity shows that it has a number of behavioral features in the spectral range $\lambda = 389$–1238.46 nm. The spectral sensitivity of such a structure begins at $\lambda = 389$ nm and rapidly increases, reaching a maximum (peak) at $\lambda = 475$ nm, where $S_\lambda = 5.49$ A/W. Then the spectral sensitivity vanishes at $\lambda = 872.7$ nm. The photosensitivity slope curve contains a number of features appearing as a step at $\lambda = 541.84$–578.56 nm and three small peaks at $\lambda = 618$, 740, and 821.8 nm. These features are caused by the presence of impurities in cadmium-sulfide layers.

Then, after its zero value at $\lambda = 872.7$ nm, the spectral sensitivity, changing sign, begins to increase and again reaches a maximum $S_\lambda = 0.4$ A/cm at $\lambda = 961.8$ nm. Then it gradually decreases to zero ($\lambda = 1042.8$ nm) and increases again (with sign reversal) to $\lambda = 1200.3$ nm followed by a decrease.

To explain such behavior of the dependence of the spectral sensitivity, the spectral distribution of the structure photovoltage (*U*) was measured (see Fig. 3). A comparison of the dependences $S_\lambda(\lambda)$ and $U(\lambda)$ shows their similar behavior. They contain specific extrema corresponding to maxima and minima at the same λ. This circumstance gives grounds to assert that the dependence $U(\lambda)$ defines the $S_\lambda(\lambda)$ shape. The appearance of a large peak ($\lambda = 475$ nm) is caused by generation and release of excess carriers without loss in the isotype n^+-CdS–*n*-CdS junction region. The

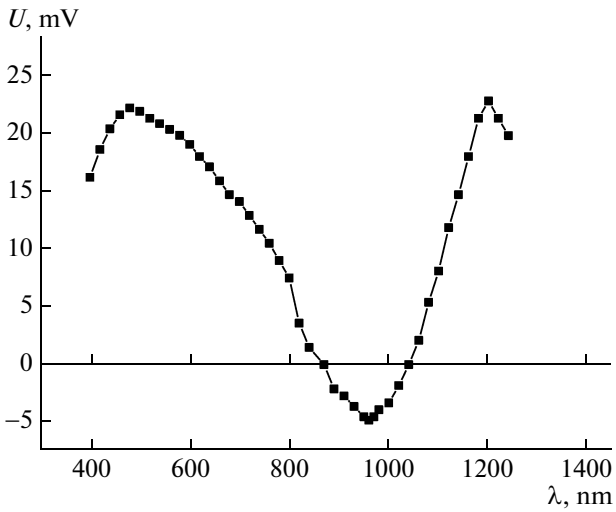

Fig. 3. Spectral distribution of the photovoltage (*U*) of the *p*-Si–*n*-CdS–n^+-CdS structure.

slope region of the large peak is explained by the fact that the photon-absorption depth increases with λ; therefore, a fraction of excess carriers does not reach the isotype junction, and all excess carriers do not reach this junction at λ = 1042.8 nm and $U = 0$ (see Fig. 3). At the same time, the decrease in U to zero is also caused by the appearance of counter diffusion and the drift flows of excess carriers mutually compensating each other. Carriers injected by the isotype n^+-CdS–n-CdS junction under the action of the photovoltage form diffusion hole flows which appear to provide electrical neutrality. The spectral sensitivity at the maximum (λ = 475 nm) significantly exceeds that of the ideal photodetector ($S_\lambda = 0.6$ A/W) [7] at a given electromagnetic-radiation wavelength (see Fig. 3). It is believed that the ideal photodetector is a photodetector in which all incident photons are absorbed and generate electron–hole pairs separated by the junction space charge without loss. The observed S_λ excess allows the conclusion that the primary photocurrent is amplified in such a structure. The mechanism of such amplification can be dual: the positive feedback or parametric mechanism [8].

The further increase in the photosensitivity after sign reversal is associated with the contribution of the p-Si–n-CdS heterojunction to photocarrier separation. The further sign change and the formation of the maximum at λ = 1200.3 nm ($S_\lambda = 0.96$ A/W) with a further decrease in the photosensitivity is explained by the dominant contribution of the p-Si–n-CdS heterojunction to the carrier diffusion and drift processes. The photosensitivity at λ = 1200.3 nm shows that the p-Si–n-CdS heterojunction efficiently separates electron–hole pairs generated by radiation. However, the spectral sensitivity at λ = 1200.3 nm is significantly lower than S_λ at λ = 475 nm. This suggests that the heterojunction efficiency is worse than that of the isotype n^+-CdS–n-CdS junction.

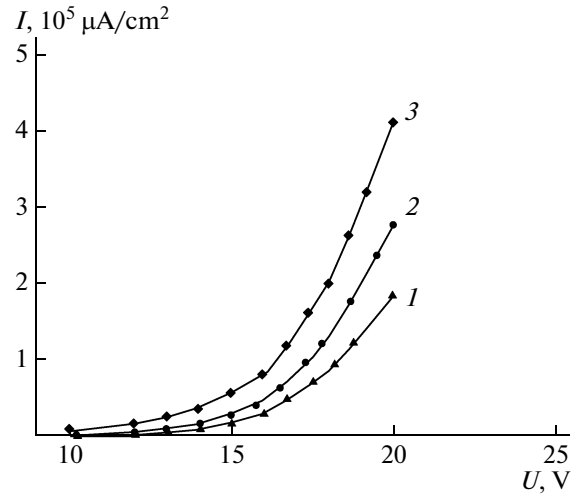

Fig. 4. Semilog current–voltage characteristic of the p-Si–n-CdS–n^+-CdS structure: (*1*) forward portion in the dark, (*2*) forward portion upon irradiation with white light with $E = 10$ lux, (*3*) forward portion under laser irradiation with λ = 0.625 nm of power $P = 100$ μW/cm^2.

Then, to prove the existence of primary photocurrent amplification, the dark and light I–V characteristics of the structure were studied (see Fig. 4). The light I–V characteristics were measured at the various illuminances E by white light and various laser irradiation powers W with a wavelength of λ = 625 nm (see table). The studies conducted show that the photocurrent amplification effect indeed takes place in the p-Si–n-CdS–n^+-CdS structure. For example, under laser irradiation with a power of $P = 10$ μW/cm^2, $S_\lambda = 2.3 \times 10^4$ A/W; under irradiation with white light with $E = 0.1$ lux, the integral sensitivity $S_{int} = 2.75 \times 10^4$ A/lm (3×10^6 A/W) at room temperature (see table). We note that the structure under study is very sensitive to

Dependences of the photocurrent (I_{ph}), integral sensitivity (S_{int}), spectral sensitivity (S_λ) on the illuminance (E_{lux}), laser irradiation power (P), and bias voltage (U)

E (lux)	U, V	I_{ph}, μA/cm^2	S_{int}, A/lm	S_{int}, A/W	P, μW/cm^2	I_{ph}, μA/cm^2	S_λ, A/W
0.1	5	148.6	14.8	0.2×10^4	10	133	13.3
	10	2354.4	235.44	2.6×10^4		2000	200
	14	17000	1700	1.87×10^5		11200	1120
	20	274500	27450	3×10^6		233560	23356
1	5	178	1.78	0.2×10^3	50	369.2	7.4
	10	3020	30.2	3.32×10^3		6075.6	121.5
	14	18000	180	1.98×10^4		38937.1	778.7
	20	310220	3102	3.4×10^5		416333	8326
10	5	184	0.184	0.2×10^2	100	456	4.56
	10	3600	3.6	4×10^2		7524	75.24
	14	21000	21	2.31×10^3		44025	440.25
	20	410500	410	4.5×10^4		448320	4483.2

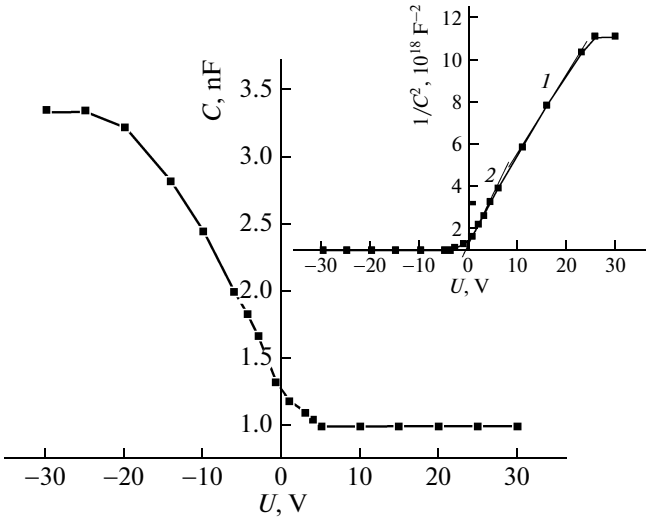

Fig. 5. Capacitance–voltage characteristic of the p-Si–n-CdS–n^+-CdS structures at the frequency $f = 10$ kHz and $T = 300$ K. The inset shows the dependence of C^{-2} on V of this structure at the frequency $f = 10$ kHz and $T = 300$ K.

low illumination levels, and has high integral and spectral sensitivities in both the intrinsic and extrinsic light absorption regions (see table). Furthermore, it was found that both S_{int} and S_λ decrease with increasing illumination level and laser irradiation power.

It is known that the injection and accumulation properties of barriers control the I–V characteristics of the structure. Therefore, the forward I–V characteristic of the structure in the dark was studied, which is shown in Fig. 1 (see the inset) on the semilogarithmic scale. Analysis of the forward I–V characteristic of the p-Si–n-CdS–n^+-CdS structure showed that it consists of four portions at room temperature.

The first, second, and fourth portions are described by the exponential dependence of the current on the voltage, analytically expressed as

$$I = I_0[\exp(qV/ckT) - 1], \qquad (1)$$

where c is the exponent, I_0 is the pre-exponential factor, q is the electron charge, k is the Boltzmann constant, T is the absolute temperature, and V is the bias voltage.

We note that c and I_0 are different for each portion. The third portion is described by the sublinear voltage dependence of the current.

Let us analyze these portions. The first portion is observed at current densities of $I \approx 10^{-7}$–4×10^{-6} A/cm^2, at which the exponent $c_1 = 1.04$ and the pre-exponential factor $I_{01} = 1.3 \times 10^{-8}$ A/cm^2. Such values are inherent to formula (1), when thermionic-emission currents flow in the structure [9].

Thermionic-emission currents take place in structures with a Schottky barrier and in metal—insulator–semiconductor (MIS) structures. The study carried out showed that the p-Si–n-CdS–n^+-CdS structure has a capacitance–voltage (C–V) characteristic typical of a MIS structure (see Fig. 5). In the structure under study, heavily compensated high-resistivity n-CdS appears as an insulator, while p-Si appears as a semiconductor. Analysis of the C–V characteristics fully confirms this. The insulator thickness d_i was determined by its capacitance $C_i = 3.35$ nF as ~0.06 μm for the structure area $S \approx 0.1$ cm^2. The calculated insulator thickness differs from the high-resistivity base thickness $w \sim 2$ μm (n-CdS). Such a difference is caused by the formation of oxide layers such as CdO_x and SO_x on the base surface and a SiO_x oxide layer on the p-Si surface during deposition of the n-CdS films. This suggests that the n-CdS film resistance is much lower than the oxide-layer resistance; therefore, the n-CdS layer capacitance does not manifest itself in measurements. The equilibrium hole concentration p_0 was determined by the flat-band capacitance and the steep portion of the C–V characteristic. To determine p_0 via the C–V characteristic, the steep portion was constructed in C^{-2}–V coordinates where it showed two slopes. By these slopes, using the known formula [10]

$$p_0 = \frac{2}{q\varepsilon_0\varepsilon_S S^2 \dfrac{d(C^{-2})}{dV}}, \qquad (2)$$

where q is the elementary charge, ε_0 is the vacuum permittivity, ε_S is the semiconductor permittivity, V_b is the potential barrier height, and S is the structure area, the equilibrium hole concentrations were determined as 3.2×10^{15} and 4×10^{14} cm^{-3}. Extrapolating the dependence $C^{-2}(V)$ to the voltage axis, the potential barrier height for p_0 in p-Si was determined as $V_b = (0.89 \pm 0.02)$ eV. The equilibrium hole concentration was also determined by the flat-band capacitance using the formula [9]

$$C_{n3} = \frac{\varepsilon_0\varepsilon_i S}{d_i + \dfrac{\varepsilon_i}{\varepsilon_S}\sqrt{\dfrac{kT\varepsilon_0\varepsilon_i}{p_0 q^2}}}, \qquad (3)$$

where ε_i is the insulator permittivity and d_i is the insulator thickness, as $p_0 \approx 1.8 \times 10^{15}$ cm^{-3}.

The values of p_0 determined by the capacitance–voltage characteristic are in good agreement with the equilibrium hole concentration, i.e., ~1.3×10^{15} cm^{-3} for p-Si.

Thus, the results obtained from the C–V characteristic confirm that the structure under study behaves as a MIS structure, and its actual structure is p-Si–n-CdS–n^+-CdS. At low current densities, thermionic currents flow in this structure. The thermionic current is described by the formula [11]

$$I = AT^2 e^{-\frac{V_b}{kT}}\left(e^{\frac{eV}{ckT}} - 1\right) = I_{01}\left(e^{\frac{eV}{ckT}} - 1\right), \qquad (4)$$

where

$$I_{01} = AT^2 e^{-\frac{V_b}{kT}}, \quad (5)$$

where A is the Richardson constant, $A = 12 \times 10^5$ A/(m^2 deg^2), V_b is the potential barrier height, V is the bias voltage, T is the absolute temperature, k is the Boltzmann constant, and c is the exponent.

Using the experimental value $I_{01} = 1.3 \times 10^{-8}$ A/cm^2 determined from the first I–V portion using expression (5), we find the potential barrier height $V_b = (0.86 \pm 0.02)$ eV which is in good agreement with the potential barrier determined by the C–V characteristic. The results obtained once again confirm that the current-flow mechanism in the first I–V portion is thermionic emission.

In the second I–V portion, in the current density range $I = (1.8 \times 10^{-6}$–$4 \times 10^{-5})$ A/cm^2, c and I_0 significantly increase and become 3.6 and 5.4×10^{-8} A/cm^2, respectively. Here electronic processes occur in the n-CdS layer. An analysis performed shows that carrier injection from the n^+–n junction to the i-layer (n-CdS) takes place and its resistance plays a significant role.

There is the known relation $M = (I_p/I_n) = \exp[-(E_{gn} - E_{gp})/kT]$ for ideal heterojunctions [12], where E_{gn} and E_{gp} are the band-gap widths of wide-gap and narrow-gap semiconductors, I_p and I_n are hole and electron currents, respectively. The quantity M shows that the current flows from the wide-gap semiconductor to the narrow-gap semiconductor [12]. It follows from the relation for M that the larger the difference between band gaps ΔE_g of these semiconductors, the stricter this relation. For example, for the heterojunction between silicon and germanium, the relation between currents flowing from Si to Ge differs by a factor of e^{-16} [12]. In the case at hand, the difference between the band gaps of Si and CdS forming the heterojunction is 1.3 eV, whereas $\Delta E_g = 0.4$ eV for Si and Ge. From this it follows that M for the p-Si–n-CdS heterojunction should be much larger, and the current in the structure under study is exclusively controlled by electron flows from n-CdS to p-Si. The above considerations are valid for ideal heterojunctions. In actual heterojunctions, surface states exist at the interface between semiconductors; hence, the relation for M can not be strictly satisfied. The surface states are formed (i) due to the difference between the lattice constants of contacting p-Si and n-CdS, which is more than 7% [13], and (ii) during the technological processes. These surface states can be recombination centers or centers of hole tunneling to the structure base. Nevertheless, we believe that the structure current is mostly controlled by electron flows from the n^+–n junction. An analysis of the second I–V portion shows that diffusion currents flow in the base, which are formed by minority excess carriers (holes) which appear from the opposite p-Si–n-CdS junction to provide the base electrical neutrality. It is known from publications that if the accumulation effect is insignificant, only the known dependences $I \propto \exp(qV/kT)$ and $I \propto \exp(qV/ckT)$ first obtained by Shockley [14] and Stafeev [15] for p–n diode structures with an ohmic contact and a significant base resistance are retained in the diffusion mode among the variety of I–V characteristics.

The expression for the diffusion current, obtained by Stafeev, is given by [15]

$$I = I_{02}\exp(qV/ckT). \quad (6)$$

Here

$$c = (2b + \cosh w/L + 1)/(b + 1), \quad (7)$$

$$I_c = (kT/q)(b\cosh(w/L))/[2(b + 1)L\rho\tan w/2L], \quad (8)$$

where $b = \mu_n/\mu_p$ is the ratio of electron and hole mobilities, w is the base thickness, ρ is the base resistivity, I_{02} is the pre-exponential factor, and L is the diffusion length of minority carriers.

Substituting the experimental value $c = 3.6$ into formula (7), we find that $L_p = 0.48$ μm, $\mu_p\tau_p = 8.8 \times 10^{-8}$ cm^2/V (the product of the hole mobility and lifetime) at $b = 38$ [16] and $w = 2$ μm. Since I_{02} is approximately equal to the current at which the base-region conductivity is twofold increased by injection, i.e., the equilibrium and nonequilibrium conductivities of thicknesses become equal, and the transition to higher injection levels occurs. Therefore, assuming that $I_{02} = 5.4 \times 10^{-9}$ A/cm^2 corresponds to the initial voltage of the second I–V portion (0.1 V), we find that the base resistivity is $\rho = 1.5 \times 10^{10}$ Ω cm.

The base ρ determined in such a way is its lower limit, and direct measurement of the film resistance shows that $\rho \approx 2.2 \times 10^{10}$ Ω cm. These values are in good agreement and point to the diffusion mechanism of current flow in the second I–V portion. The validity of this current flow mechanism is also confirmed by the other estimate using the product $\mu_p\tau_p = 8.8 \times 10^{-8}$ cm^2/V. To this end, relaxation curves were measured in the absence of bias. By the rise and slope of these curves, the relaxation-time constants were determined as $\tau = 7 \times 10^{-8}$ and 1.2×10^{-7} s. Then, assuming that these relaxation-time constants are hole lifetimes, from the product $\mu_p\tau_p$, we obtain the hole mobilities $\mu_p = 1.25$ and 0.9 cm^2/(V s), respectively. The obtained hole mobilities are in good agreement with the published data ($\mu_p = 7$–8 cm^2/(Ω cm)) [16], bearing in mind that the base of the structure under study is a polycrystalline material.

Thus, this study once again confirms that the current in the structure is of the diffusion type when the accumulation process is insignificant. In this case, excess holes represent the main component of the diffusion current. As seen in Fig. 1, there is a portion with curvature between the second and third I–V portions. The existence of this portion shows that holes are accumulated near the isotype n^+-CdS–n-CdS junction, which is also indicated by the appearance of the sublinear portion behind it.

According to the published data [17–19], the sublinear I–V portion is observed when diffusion and drift flows are directed towards each other. Such a phenomenon takes place if excess carrier accumulation in the structure dominates. In the p-Si–n-CdS–n^+-CdS structure under study, the hole accumulation process occurs near the p-Si–n-CdS heterojunction. As negative bias is applied to the n^+-CdS layer of the structure, electrons are injected to the base; at the same time, to provide electrical neutrality, the same number of holes arrives at the base from the opposite junction. These holes form the diffusion current in the base. As a result, their concentration exceeds the equilibrium hole concentration in the near-contact region of the heterojunction. The accumulation effect takes place when the p-Si–n-CdS heterojunction is opaque to holes, which explains the appearance of the sublinear portion in the I–V characteristic. In this case, the hole concentration gradient will become positive ($dp/dx > 0$). Physically, this means that the diffusion and drift currents are directed towards each other. In this case, the I–V structures are described by the following analytical expression [17, 18]

$$V = V_0 \exp(aIw), \tag{9}$$

where

$$a = 1/2qD_nN_t. \tag{10}$$

In expression (9), the pre-exponential factor V_0 is given by

$$V_0 = \frac{D_{\text{eff}}}{\mu_p}\frac{b+1}{b(b\gamma+b+1)}\frac{p_{\text{Sb}}^2}{N_t p(d)},$$

where D_{eff} is the bipolar diffusion coefficient, $\gamma = N_t/p_{1t}$ is the trapping factor, p_{Sb} is the excess hole concentration near the anode (near the n^+–n junction), and $p(w)$ is the excess hole concentration near the cathode (p–n junction). In formula (10), D_n is the electron diffusion coefficient, N_t is the concentration of trapping levels, and I is the current density.

Using expressions (9) and (10), the concentration of deep trapping centers was determined as $N_t = 2 \times 10^{10}$ cm^{-3} at the following parameters: $\mu_n \approx 30$ cm^2/(V s) and $w = 2$ μm. Let us assume that this deep trapping level has a high trapping cross section for holes and its population modulation is a controlling factor affecting the ambipolar drift velocity v_a [17–19]. In this case, the expressions for the ambipolar drift velocity and diffusion become simpler: $D_{\text{eff}} \approx D_p$ and $v_a \approx aID_{\text{eff}}$. Using these expressions, v_a was determined from the sublinear I–V portion as ~250 cm/s. Thus, the estimation performed yields a rather high value for v_a. This shows that the ambipolar mobility in the sublinear I–V portion is subject to strong modulation.

As noted above, the fourth I–V portion is described by the exponential dependence $I = I_{04}\exp(qV/c_4kT)$, where $c_4 = 68$ and $I_{04} = 1.9 \times 10^{-7}$ A/cm^2. Substituting these experimental data into formulas (7) and (8), we determine the ratio of the base thickness to the hole diffusion length as $w/L_p = 8.5$ and the base resistivity as $\rho = 1.9 \times 10^7$ Ω cm. The values L_p and ρ estimated from the fourth I–V portion differ significantly from the same values calculated from the second portion. This difference is explained by changes in the base properties with the current density in the structure. These estimates show that the diode structure at current densities at which the fourth I–V portion is observed can be attributed to the class of "long" enough diodes [20]. As is known, the current in long enough diodes is mainly controlled by the drift mechanism.

The study of the light I–V characteristics for various illuminances by white light and under laser irradiation of various powers (see table) show that they are identical in shape and have identical dependences of the current on the bias voltage (Fig. 4); the highest integral and spectral sensitivities are within the fourth I–V portion. This allows us to argue that the ambipolar mobility modulation is the major factor in the primary photocurrent amplification. The ambipolar mobility modulation occurs due to deep trapping-level depletion [8].

4. CONCLUSIONS

An injection photodiode based on the p-Si–n-CdS–n^+-CdS structure was developed. It was found that the p-Si–n-CdS heterojunction has a low surface-state density at the interface, which points to its high rectification factor. It was shown that the light and dark current–voltage characteristics of the structure have identical behavior features. Therewith, it was revealed that systematic features of the voltage dependence of the current vary with the structure current density. It was found that the base properties vary as the structure current density increases, which causes a change in the diffusion length of minority carriers and the mechanism of current transport in the structure under study. As a result of these processes, the integral and spectral sensitivities of the structure under study also change. It was found that the mode of long enough diodes is implemented in the structure at current densities of $I = 10^{-2}$–5×10^{-4} A/cm^2; in this case, S_{int} and S_λ sharply increase. For example, $S_{\text{int}} = 2.8 \times 10^4$ A/lm (3×10^6 A/W) at an illuminance of $E = 0.1$ lux and $S_\lambda = 2.3 \times 10^4$ A/W under laser irradiation with $\lambda = 625$ nm. The obtained integral and spectral sensitivities are record for room temperature.

Finally, we can conclude that the mechanism of the primary photocurrent amplification at high current densities is mainly controlled by ambipolar carrier-mobility modulation.

REFERENCES

1. I. M. Koldaev, V. V. Losev, and B. M. Orlov, Sov. Phys. Semicond. **18**, 823 (1984).

2. Sh. A. Mirsagatov and A. K. Uteniyazov, Tech. Phys. Lett. **38**, 34 (2012).
3. Sh. A. Mirsagatov, R. R. Kabulov, and M. A. Makhmudov, Semiconductors **47**, 825 (2013).
4. Sh. A. Mirsagatov, O. K. Ataboev, and B. N. Zaveryukhin, Fiz. Inzhen. Poverkhn. **11** (1), 4 (2013).
5. A. S. Saidov, A. Yu. Leiderman, Sh. N. Usmonov, and K. T. Kholikov, Semiconductors **43**, 416 (2009).
6. E. Frish, *Optical Methods of Measurements* (Leningr. Gos. Univ., Leningrad, 1976), pt. 1, p. 126 [in Russian].
7. A. Ambrozyak, *Construction and Technology of Semiconductor Photoelectrical Devices* (Sov. Radio, Moscow, 1970), p. 392 [in Russian].
8. I. M. Vikulin, Sh. D. Kurmashev, and V. I. Stafeev, Semiconductors **42**, 112 (2008).
9. S. M. Sze, *Physics of Semiconductor Devices* (Wiley–Interscience, New York, Chichester, Brisbane, Toronto, Singapore, 1981), Vol. 1, p. 386.
10. V. G. Georgiu, *Voltage-Capacity Measurements of Semiconductor Parameters* (Shtiintsa, Kishinev, 1987), p. 15 [in Russian].
11. P. G. Oreshkin, *Physics of Semiconductors and Insulators* (Vyssh. Shkola, Moscow, 1977), p. 173 [in Russian].
12. I. M. Vikulin and V. I. Stafeev, *Physics of Semiconductor Devices* (Sov. Radio, Moscow, 1980), p. 36 [in Russian].
13. A. Milnes and D. Feught, *Heterojunctions and Metal Semiconductor Junctions* (Academic Press, New York, 1972; Mir, Moscow, 1975), p. 425.
14. W. Shockley, Bell Syst. Techn. J. **28**, 4351 (1949).
15. V. I. Stafeev, Sov. Tech. Phys. **3**, 1502 (1958).
16. V. I. Fistul', *Physics and Chemistry of Solids* (Metallurgiya, Moscow, 1995), vols. 1, 2 [in Russian].
17. A. Yu. Leiderman and P. M. Karageorgy-Alkalaev, Solid State Commun. **25**, 781 (1978).
18. E. I. Adirovich, P. M. Karageorgij-Alkalaev, and A. Yu. Leiderman, *Double Injection Currents in Semiconductors* (Sov. Radio, Moscow, 1978), p. 126 [in Russian].
19. P. M. Karageorgij-Alkalaev and A. Yu. Leiderman, *Photosensitivity in Semiconductor Structures with Deep Impurities* (Fan, Tashkent, 1981), p. 200 [in Russian].
20. V. V. Osipov and V. I. Stafeev, Sov. Phys. Semicond. **1**, 1486 (1967).

Translated by A. Kazantsev